ISSN 0031-918X, Physics of Metals and Metallography, 2021, Vol. 122, No. 9, pp. 915–922. © Pleiades Publishing, Ltd., 2021.
Russian Text © The Author(s), 2021, published in Fizika Metallov i Metallovedenie, 2021, Vol. 122, No. 9, pp. 984–992.

STRENGTH AND PLASTICITY

Structure and Properties of New Wrought Al–Cu–Y- and Al–Cu–Er-Based Alloys

S. M. Amer[a, b], R. Yu. Barkov[a], A. S. Prosviryakov[a], and A. V. Pozdniakov[a, *]

[a] *National University of Science and Technology MISiS, Moscow, 119991 Russia*

[b] *Mining, Metallurgy and Petroleum Engineering Department, Faculty of Engineering, Al-Azhar University, Cairo, 11884 Egypt*

**e-mail: pozdniakov@misis.ru*

Received February 8, 2021; revised April 2, 2021; accepted April 13, 2021

Abstract—The structure and properties of new wrought aluminum Al–4.5Cu–1.6Y–0.9Mg–0.6Mn–0.2Zr–0.1Ti–0.15Fe–0.15Si and Al–4.0Cu–2.7Er–0.8Mg–0.8Mn–0.2Zr–0.1Ti–0.15Fe–0.15Si alloys are studied. After homogenization and rolling, the structure is formed, which consists of the aluminum-based solid solution strengthened with fine $Al_3(Zr,Er)$, $Al_3(Zr,Y)$, and $Al_{20}Cu_2Mn_3$ phase particles and compact thermally stable phases of solidification origin 1–5 μm in size. The recrystallization after rolling occurs at temperatures above 350°C. As the annealing temperature increases from 400 to 550°C, the recrystallized grain size increases from 6–8 to 10–12 μm. At temperatures of 150–180°C, the hardness increases after 2-h annealing; this is related to the occurrence of aging, and the analogous effect was observed for the cast alloys of these systems. The yield strength of the Y-containing alloy subjected to 6-h annealing at 150°C is 405 MPa; in this case, the relative elongation is 4.5%. As the annealing temperature increases to 210°C, the yield strength of the both alloys decreases to 300 MPa, whereas the relative elongation remains unchanged. In the case of the alloys quenched after rolling and subsequently aged at 210°C, the yield strength of 264–266 MPa and ultimate tensile strength of 356–365 MPa are reached at a relative elongation of 11.3–14.5%. As a result, the new wrought Al–Cu–Y- and Al–Cu–Er-based alloys provide competition for the available industrial alloys.

Keywords: aluminum alloys, rare-earth metals, yttrium, erbium, dispersoids, microstructure, heat treatment, hardness, strength, long-term strength

DOI: 10.1134/S0031918X21080020

INTRODUCTION

The aluminum Al–Cu-base alloys are characterized by a sufficiently high strength at both room and high temperatures and very low manufacturability upon casting [1–6]. The high manufacturability upon casting, in particular, the low solidification cracking susceptibility is of importance for both shaped castings and semicontinuous casting ingots [2–7]. The alloying with eutectic-forming elements, such as Fe, Si, Mn, Ni, and Ca, favors an increase in the manufacturability upon casting [3–9]. However, often, in reaching a low solidification cracking susceptibility, the alloys have a highly heterogeneous structure and low plasticity [6], which, in turn, makes the preparation of wrought half-finished products difficult. An alternative variant is the search for new alloying systems, for which the structure with fine phases of solidification origin and the narrow solidification range might be combined. The Al–Cu–Ce- [10, 11], Al–Cu–Y- [12, 13], Al–Cu–Er- [13, 14], and Al–Ca-based [8, 9, 15] alloys are among such systems. The distinctive feature of the yttrium- and erbium-containing alloys containing also zirconium and/or scandium is the possibility of precipitation strengthening in the course of annealing of ingots [16–36]. Low yttrium and erbium additions to the aluminum-based alloy [16–23] and to magnalium [24–28] increase the strengthening effect during annealing of ingots and restrain the softening during annealing after rolling at the expense of the increase in the density of dispersoid precipitates formed during the first heat treatment. Erbium efficiently modifies the grain structure [24–26, 30] and decreases the hot-brittleness of the Al–5Cu alloy [31]. The ternary Al–Cu–Y and Al–Cu–Er alloys [12–14] are characterized by narrow solidification range, and the phases of solidification origin are characterized by small sizes and high thermal stability. The alloying with zirconium [32, 33] and jointly zirconium and manganese [34, 35] leads to a substantial increase in the strength characteristics of alloys after deformation. The manganese addition leads to the formation of $Al_{25}Cu_4Mn_2Er$ [34] and $Al_{25}Cu_4Mn_2Y$ [35] phases of solidification origin. Iron impurity is dissolved in the phases of solidification origin and does not change their morphology, whereas silicon leads to the formation of sufficiently compact $Al_3Er_2Si_2$ and $Al_{11}Cu_2Y_2Si_2$ [36, 37] phases. The complexly alloyed Al–Cu–Y- and Al–Cu–Er-based alloys with magnesium, manganese, zirconium, and titanium additions exhibit the adequate manufacturability upon casting, high

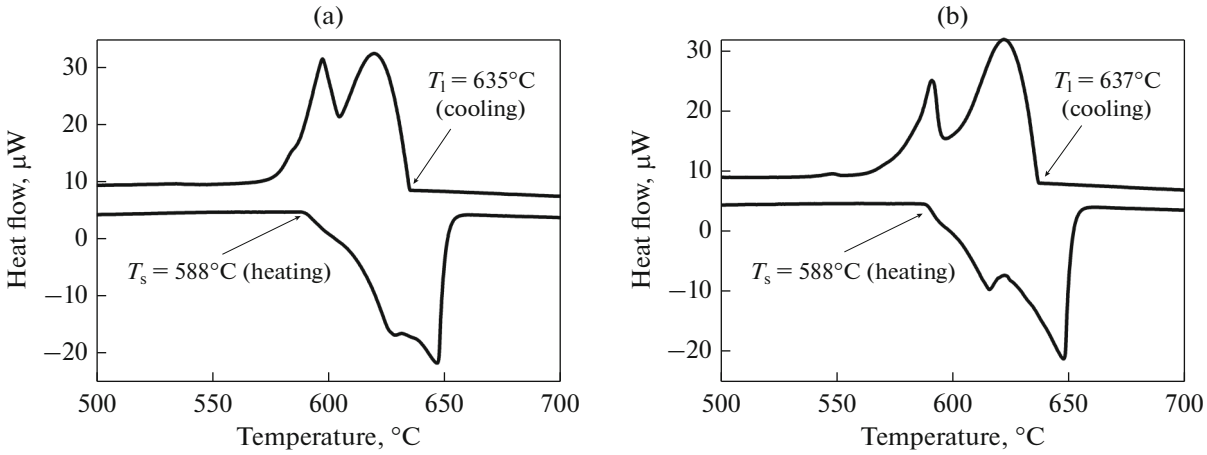

Fig. 1. DSC curves for the (a) AlCuYMg and (b) AlCuErMg alloys.

strength, and mechanical properties at elevated temperatures [38]. The main disadvantage of these alloys is not high plasticity [38].

This study is aimed at the investigation of the structure and properties of new wrought aluminum Al–Cu–Y- and Al–Cu–Er-based alloys with the low contents of main alloying elements, such as copper, yttrium, erbium, zirconium, manganese, and titanium, which also contain magnesium and iron and silicon impurities.

EXPERIMENTAL

The Al–4.5Cu–1.6Y–0.9Mg–0.6Mn–0.2Zr–0.1Ti–0.15Fe–0.15Si (AlCuYMg) and Al–4.0Cu–2.7Er–0.8Mg–0.8Mn–0.2Zr–0.1Ti–0.15Fe–0.15Si (AlCuErMg) (wt %) alloys were melted at 780°C using a resistance furnace, A7 aluminum, Mg90 magnesium, and Al–51.7Cu, Al–10Y, Al–8Er, Al–10Mn, Al–5Zr, and Al–5Ti–1B master alloys and were cast into a copper water-cooled mold with the internal hollow 20 mm × 40 mm × 120 mm in size. The compositions studied in this work differ from analogous casting alloys [38] in the lower copper, yttrium, erbium, zirconium, manganese, and titanium contents. The density of alloys was determined by hydrostatic weighing method. A Labsys Setaram differential scanning calorimeter (DSC) was used to determine the solidus and liquidus temperatures. The homogenizing annealing was performed at 575°C for 3 h. After homogenizing annealing, the alloys were rolled at 500°C and room temperature to thicknesses of 10 and 1 mm, respectively. After deformation, the alloys were annealed at 100–550°C for different times. The aging at 150–210°C for 0.5–6 h was performed after deformation and subsequent quenching from 575°C; the holding time at this temperature was 15 min. Metallographic studies and identification of phases were performed by light microscopy (LM) using a Zeiss optical microscope and scanning electron microscopy (SEM) using a TESCAN VEGA 3LMH scanning electron microscope. The Vickers hardness (H_V) was measured in accordance with the standard procedure using the 5-kg load. Tensile tests were carried out using a Zwick/Roll Z250 universal testing machine. Total corrosion tests were performed using artificial sea water.

RESULTS AND DISCUSSION

The liquidus temperature of the alloys under study is 635–637°C (Fig. 1) and is higher by 3–5°C than that of analogous casting alloys [38]. The liquidus temperature is determined, in accordance with the ternary phase diagrams [39, 40], by the contents of the main additions, such as copper, yttrium, and erbium. The solidus temperature is almost unchanged and is 588°C (see Fig. 1). The alloys are characterized by the narrow solidification range, namely, 47–49°C, which determines the high manufacturability upon casting. The density of the studied AlCuYMg and AlCuErMg alloys is 2.81 and 2.86 g/cm^3, respectively; these values are by 0.2–0.3 g/cm^3 lower than that of casting alloys containing a great amount of alloying additions [38].

Figure 2 shows the microstructure of the alloys in the cast state. The decrease in the concentration of the main modifier, namely, titanium, to 0.1% leads to the formation of grains 80–100 μm in size in both alloys (Figs. 2a, 2b). For comparison, the grain size of the Ti-free Al–Cu–Y–Zr alloy is ~190 μm, whereas the grain size of the AlCuErMg alloy with 0.15Ti is 25 μm. The decrease in the concentration of the main alloying elements does not affect the phase composition of the alloys (Figs. 2b, 2d and data of [38]). The microstructure consists of the aluminum solid solution, fine eutectic, and intermetallics formed by manganese, magnesium, silicon, and copper additions (Figs. 2b, 2d). Iron does not form phases typical of aluminum alloys.

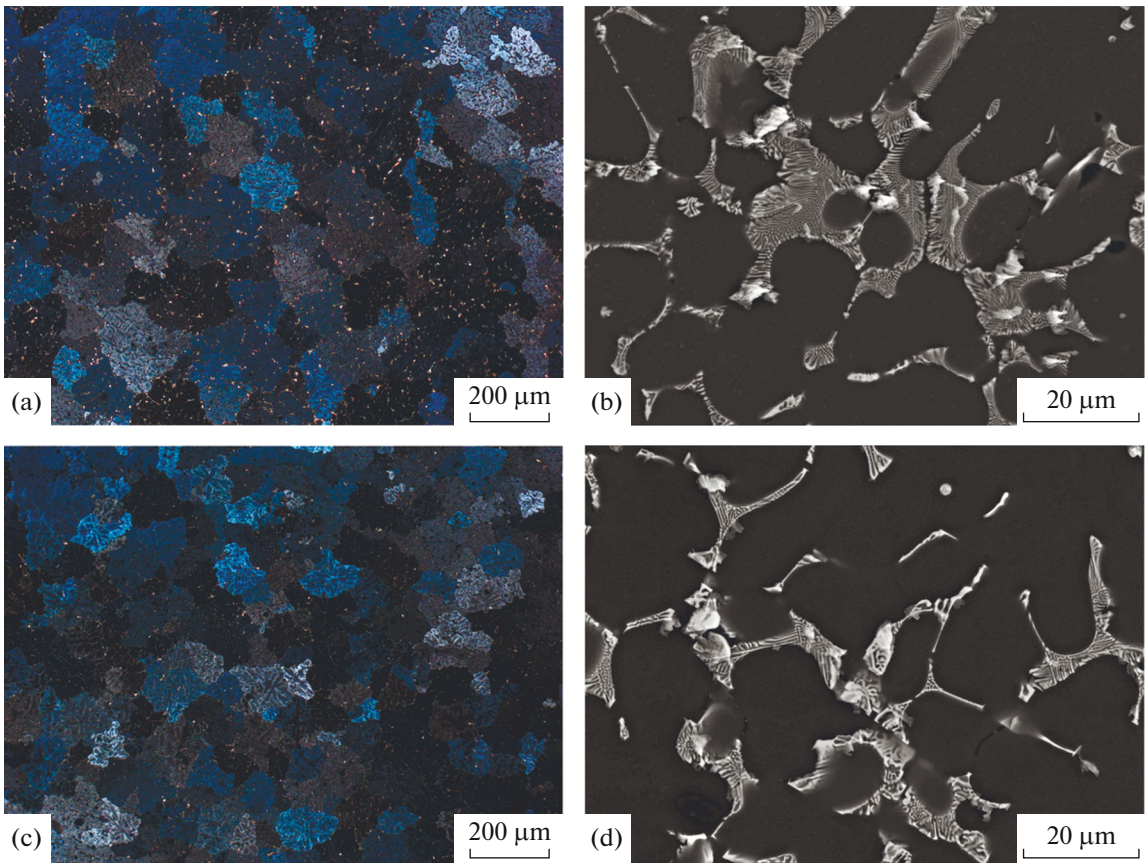

Fig. 2. (a,c) Grain structure (LM) and (b, d) microstructure (SEM) of the (a, b) AlCuYMg and (c, d) AlCuErMg alloys in the cast state.

Before quenching, the ingots of the alloys were annealed at 575°C for 3 h in accordance with the regime used for casting alloys [38]. The dissolution of nonequilibrium excess of phases of solidification origin leads to the fact that the copper and magnesium concentrations in the solid solution increase to 2.1–2.2 and 0.9–1.0%, respectively. In the course of annealing, the fragmentation and spheroidization of the phases of solidification origin take place (Figs. 3f, 3b), which partially are crushed and elongate along the deformation direction in the course of rolling (Figs. 3c, 3d). As a result, their size is 1–5 μm. Together with the homogenization processes, $Al_3(Zr,Er)$, $Al_3(Zr,Y)$, and $Al_{20}Cu_2Mn_3$ phase dispersoids precipitate from the solid solution supersaturated with zirconium, yttrium, erbium, and manganese [34, 35]. SEM images of the microstructure (Fig. 3) show fine bright inclusions in the aluminum solid solution, which correspond to the described phases.

Deformed sheets were annealed at 100–550°C in order to determine the recrystallization temperature range and to analyze changes in the hardness (Fig. 4). For both alloys, the annealing at temperatures below 350°C retains the nonrecrystallized structure. In this case, the hardness first (at temperatures below 150°C) slightly increases and, then, decreases. The increase in the hardness is likely to be related to occurred aging; the analogous effect was observed for the magnesium-free alloys of the same systems [34, 35]. The softening occurs at the expense of polygonization processes, and recrystallized grains are found after annealing at 400°C (inset in Fig. 4). In this case, the recrystallized grain size in both alloys is 6–8 μm. The increase in the annealing temperature to 550°C leads to the grain growth to 10–12 μm. In this case, the hardness is unchanged and is 65–68 HV.

Figure 5 shows the dependences of the hardness of wrought alloys on the annealing time at low temperatures. As was noted above, at temperatures close to 150°C, the slight strengthening occurs during first hours of annealing. As the temperature increases to 180°C, the softening is observed after 1-h holding, which is related to the occurrence of polygonization. In the course of annealing at 210°C, the hardness decreases after 3-h holding and remains unchanged at the holding time increases to 6 h. In this case, two opposite processes occur; these are the strengthening related to aging and softening determined by recovery and polygonization. Table 1 gives results of tensile tests

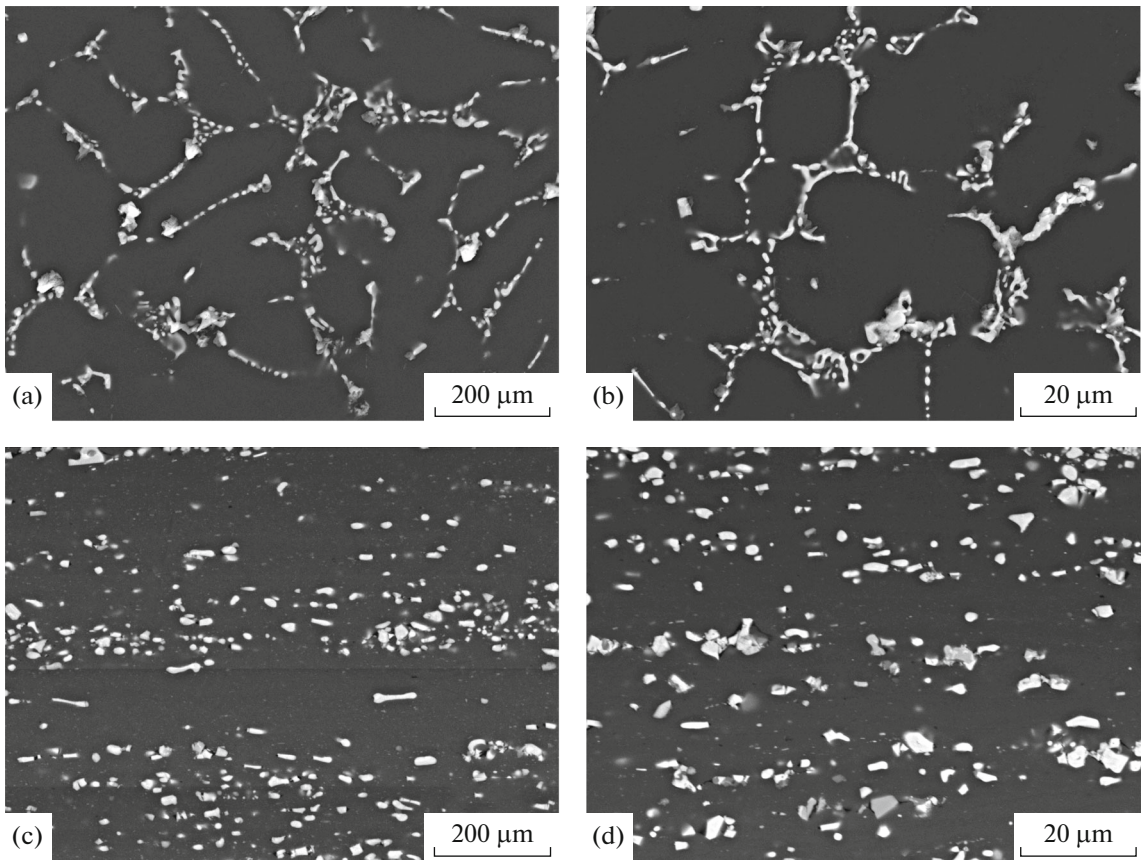

Fig. 3. Microstructure of the (a, c) AlCuYMg and (b, d) AlCuErMg alloys subjected to (a, b) annealing at 575°C for 3 h and (c, d) subsequent rolling.

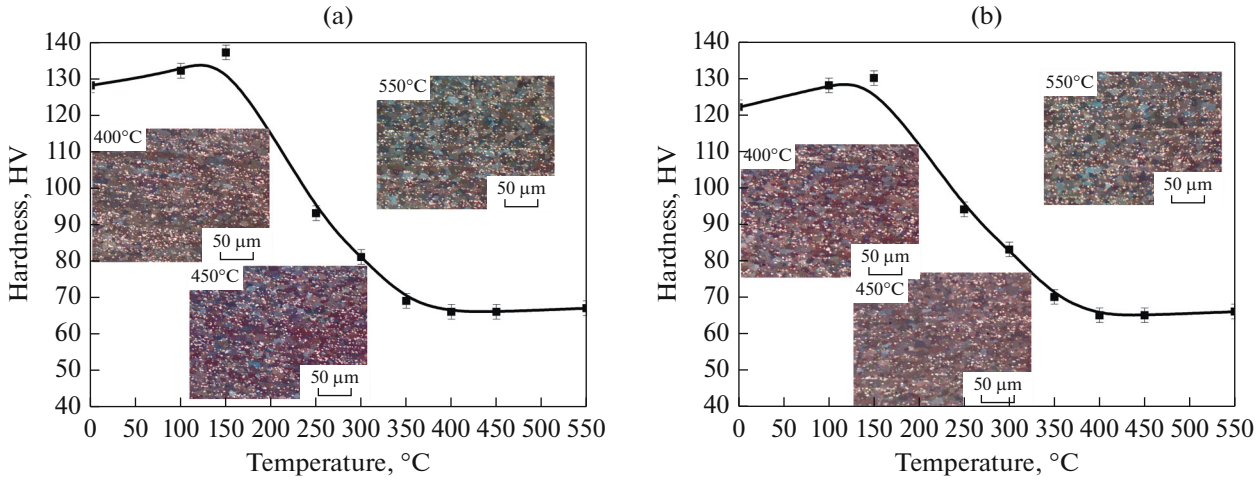

Fig. 4. Dependences of the hardness H_V on the temperature of 1 h annealing of the rolled (a) AlCuYMg and (b) AlCuErMg alloys.

of the alloys in the strained and annealed state. The yield strength of the both alloys in the strained state is 380–390 MPa and the relative elongation is 1.8–2.4%. In this case, the increase in the yield strength during annealing at 150°C is found only for the AlCuYMg alloy. After 6-h annealing, the yield strength increases from 380 to 405 MPa; the plasticity also increases from 1.8 to 4.5%. During tensile tests, the hardness and yield strength demonstrate different sensitivity to structural changes. The analogous effect was noted for the magnesium-free alloys having the close composition [34, 35]. The increase in the annealing tempera-

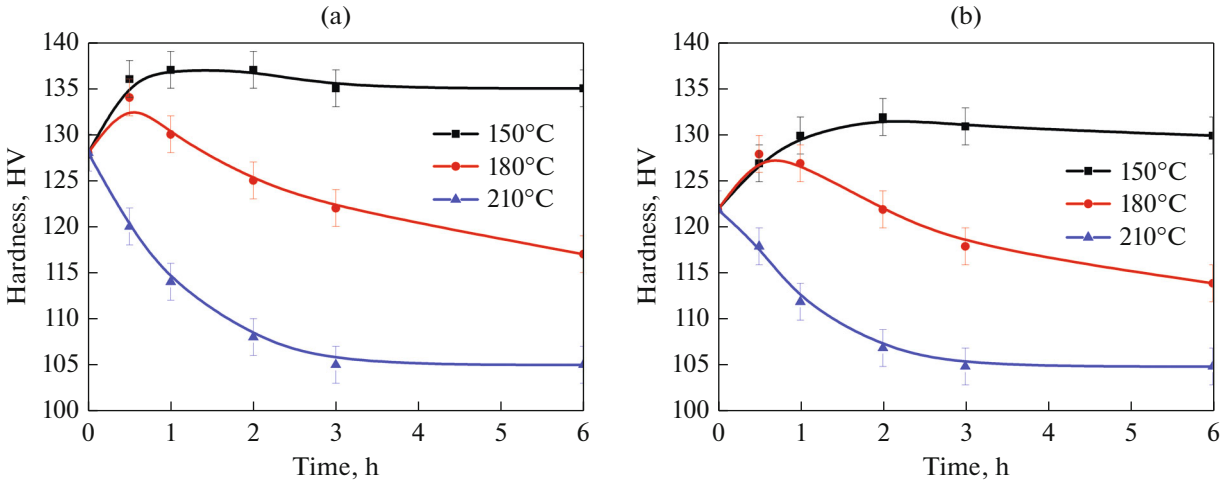

Fig. 5. Dependences of the hardness H_V of the (a) AlCuYMg and (b) AlCuErMg deformed alloys on the annealing time.

ture to 210°C leads to the decrease in the yield strength to ~300 MPa, whereas, in this case, the elongation remains not high.

After rolling, the alloys were quenched from 575°C after 15-min holding at this temperature and aged at 150, 180, and 210°C. Figure 6 shows the dependences of the hardness (H_V) on the time of aging of sheets after quenching. The observed dependences are qualitatively analogous in the fact that they are obtained upon aging of analogous casting alloys [38]. The hardness increases during aging from 64–66 to 105–115 HV. The recrystallized structure formed in the alloys (inset in Fig. 6) allows the plasticity of the alloys to be substantially increased. According to tensile test data, the

Table 1. Mechanical characteristics (tensile tests) of the alloys in strained and annealed states

State	$\sigma_{0.2}$, MPa	σ_u, MPa	δ, %
	AlCuYMg		
Strained	380 ± 4	381 ± 5	1.8 ± 0.5
Annealing at 150°C for 1 h	390 ± 5	422 ± 3	4.8 ± 0.4
Annealing at 150°C for 6 h	405 ± 3	432 ± 1	4.5 ± 1.2
Annealing at 180°C for 0.5 h	382 ± 4	416 ± 2	4.5 ± 0.2
Annealing at 180°C for 6 h	327 ± 3	360 ± 4	4.0 ± 0.9
Annealing at 210°Cfor 0.5 h	325 ± 4	358 ± 4	1.5 ± 0.5
Annealing at 210°Cfor 2 h	303 ± 2	330 ± 4	4.4 ± 0.8
	AlCuErMg		
Strained	391 ± 8	401 ± 10	2.4 ± 0.8
Annealing at 150°C for 1 h	370 ± 3	405 ± 2	4.2 ± 0.2
Annealing at 150°C for 6 h	376 ± 4	409 ± 7	4.5 ± 1.2
Annealing at 180°C for 0.5 h	358 ± 4	398 ± 2	6.2 ± 0.5
Annealing at 180°C for 6 h	316 ± 2	348 ± 2	4.0 ± 1.4
Annealing at 210°C for 0.5 h	320 ± 1	345 ± 4	2.7 ± 0.5
Annealing at 210°C for 2 h	295 ± 5	327 ± 2	5 ± 1
	D16		
Cold-worked and annealed sheet [41]	230–360	365–475	8–13
Rod [42]	325–345	450–470	8–10
	AK4-1		
Rod [42]	335	390	6

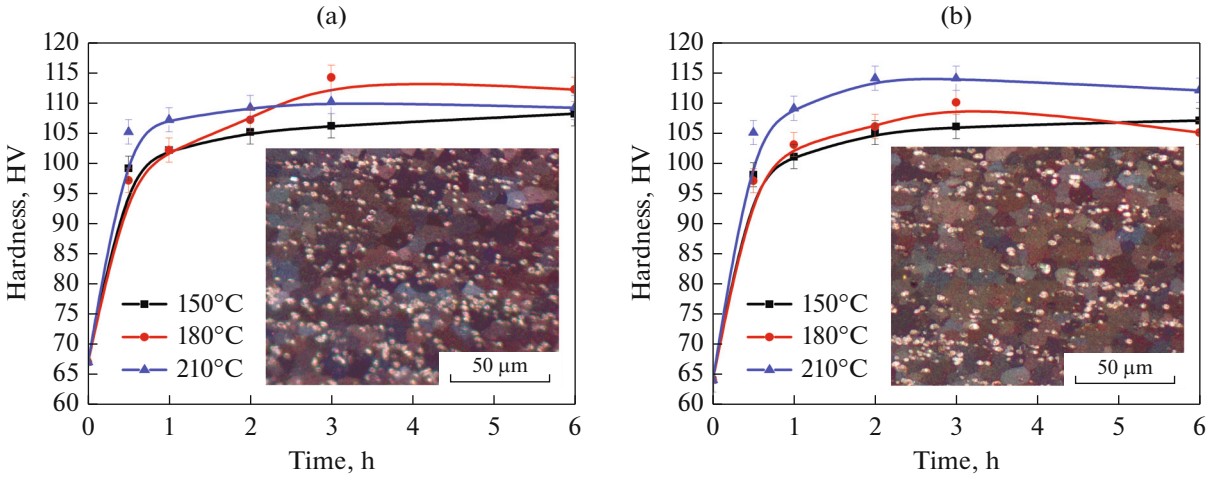

Fig. 6. Dependences of the hardness H_V of the (a) AlCuYMg and (b) AlCuErMg sheet alloys after quenching from 575°C after 15-min holding on the aging time.

relative elongation after aging at 210°C for 3 h is 11.3–14.5% (Table 2). In this case, the yield strength is 264–266 MPa, whereas the ultimate tensile strength is 356–365 MPa. For comparison, the yield strength of the wrought D16 alloy in the form of sheets in the hard-down and annealed states is 230–360 MPa; its ultimate tensile strength is 365–475 MPa and the relative elongation is 8–13%; the alloy in the form of rods [42] exhibits a yield strength of 325–345 MPa, an ultimate tensile strength of 450–470 MPa, and a relative elongation of 8–10%. The yield strength of recrystallized rods is 265 MPa [42] and their ultimate tensile strength is 410 MPa at a relative elongation of 12%. In this case, the manufacturability upon casting of the D16 alloy is substantially lower than that for the compositions under study. The wrought AK4-1 alloy characterized by the high heat resistance [42], which is prepared in the form of rods, exhibits a yield strength equal to 335 MPa and the ultimate tensile strength equal to 390 MPa at a relative elongation of 6%. Thus, the new wrought Al–Cu–Y- and Al–Cu–Er-based alloys can provide competition for the available industrial alloys.

It is known that the aluminum—copper alloys corrode. In this study, we performed a simplified estimation of the corrosion resistance in determining the total corrosion resistance in artificial sea water. After the tests, the yield strength of the AlCuYMg alloy decreases from 405 to 374 MPa, whereas the relative elongation decreases from 4.5 to 3% (Table 3). The decrease in the yield strength of the AlCuErMg alloy is less pronounced.

Table 2. Mechanical characteristics (tensile tests) of alloys subjected to rolling and subsequent quenching from 575°C after 15-min holding and aging at 210°C for 3 h

Alloy	$\sigma_{0.2}$, MPa	σ_u, MPa	δ, %
AlCuYMg	266 ± 2	365 ± 1	14.5 ± 0.5
AlCuErMg	264 ± 2	356 ± 1	11.3 ± 1.5
D16 (recrystallized)	265	410	12

Table 3. Mechanical characteristics of the alloys subjected to rolling and subsequent annealing at 150°C for 6 h determined by tensile tests before and after total corrosion tests

Alloy	Before corrosion tests			After corrosion tests		
	$\sigma_{0.2}$, MPa	σ_u, MPa	δ, %	$\sigma_{0,2}$, MPa	σ_u, MPa	δ, %
AlCuYMg	405 ± 3	432 ± 1	4.5 ± 1.2	374 ± 3	395 ± 5	3 ± 1
AlCuErMg	376 ± 4	409 ± 7	4.5 ± 1.2	365 ± 5	388 ± 6	2.7 ± 1.2

CONCLUSIONS

The structure and properties of new wrought aluminum Al–Cu–Y- and Al–Cu–Er-based compositions alloyed with zirconium, manganese, magnesium, and titanium and containing iron and silicon impurities were studied. The alloys are characterized by the narrow solidification range equal to 47–49°C, which ensures the high manufacturability upon casting. The density of the AlCuYMg and AlCuErMg alloys under study is 2.81 and 2.86 g/cm^3, respectively. After homogenizing annealing and rolling, the structure, which consists of the aluminum solid solution strengthened with fine $Al_3(Zr,Er)$, $Al_3(Zr,Y)$, and $Al_{20}Cu_2Mn_3$ phase particles and the compact thermally stable phases of solidification origin 1–5 μm in size, forms. The softening in the course of annealing performed after rolling occurs at the expense of polygonization processes at temperatures below 350°C, whereas the recrystallization occurs at the higher temperatures. After annealing at 400°C, the grain size is 6–8 μm and increases to 10–12 μm after 1-h annealing at 550°C. At temperatures of 150–180°C, the hardness slightly increases; this is related to the aging. The analogous effect was found for the casting alloys of these systems. The yield strength of the AlCuYMg alloy subjected to rolling and subsequent 6-h annealing at 150°C is 405 MPa at a relative elongation of 4.5%. The increase in the annealing temperature to 210°C leads to the decrease in the yield strength to 300 MPa, whereas the relative elongation remains unchanged. The plasticity of the alloy subjected to rolling and subsequent quenching and aging at 210°C substantially increases to 11.3–14.5%; the yield strength and ultimate tensile strength are 264–266 and 356–365 MPa, respectively. As a result, the new wrought Al–Cu–Y- and Al–Cu–Er-based alloys can provide competition for the available industrial alloys.

ACKNOWLEDGMENT

The researcher S.M. Amer is funded by a partial scholarship from the Ministry of Higher Education of the Arab Republic of Egypt.

FUNDING

This study was supported by the Russian Science Foundation, project no. 19-79-10242.

REFERENCES

1. *GOST* (State Standard) *1583–93: Aluminum Casting Alloys. Specifications* (Izd. Standartov, Moscow, 1997) [in Russian].
2. M. V. Glazoff, V. S. Zolotorevsky, and N. A. Belov, *Casting Aluminum Alloys* (Elsevier, Amsterdam, 2007).
3. *GOST* (State Standard) *4784–97: Aluminum and Wrought Aluminum Alloys. Grades* (Izd. Standartov, Moscow, 2000) [in Russian].
4. I. I. Novikov, *Hot Brittleness of Non-Ferrous Metals and Alloys* (Nauka, Moscow, 1966) [in Russian].
5. V. S. Zolotorevskiy and A. V. Pozdniakov, "Determining the hot cracking index of Al–Si–Cu–Mg casting alloys calculated using the effective solidification range," Int. J. Cast Met. Res. **27** (4), 193–198 (2014).
6. V. S. Zolotorevskii, A. V. Pozdnyakov, and A. Yu. Churyumov, "Search for promising compositions for developing new multiphase casting alloys based on Al–Cu–Mg matrix using thermodynamic calculations and mathematic simulation," Phys. Met. Metallogr. **113**, 1052–1060 (2012).
7. D. G. Eskin, Suyitno, and L. Katgerman, "Mechanical properties in the semi-solid state and hot tearing of aluminum alloys," Prog. Mat. Sci. **49**, 629–711 (2004).
8. N. A. Belov, E. A. Naumova, T. A. Bazlova, and E. V. Alekseeva, "Structure, phase composition, and strengthening of cast Al–Ca–Mg–Sc alloys," Phys. Met. Metallogr. **117**, 188–194 (2016).
9. P. K. Shurkin, N. A. Belov, A. F. Musin, and M. E. Samoshina, "Effect of calcium and silicon on the character of solidification and strengthening of the Al–8% Zn–3% Mg alloy," Phys. Met. Metallogr. **121**, 135–142 (2020).
10. N. A. Belov, A. V. Khvan, and A. N. Alabin, "Microstructure and phase composition of Al–Ce–Cu alloys in the Al-rich corner," Mater. Sci. Forum **519–521**, 395–400 (2006).
11. N. A. Belov and A. V. Khvan, "The ternary Al–Ce–Cu phase diagram in the aluminum-rich corner," Acta Mater. **55**, 5473–5482 (2007).
12. A. V. Pozdniakov and R. Yu. Barkov, "Microstructure and materials characterisation of the novel Al–Cu–Y alloy," Mater. Sci. Technol. **34** (12), 1489–1496 (2018).
13. S. M. Amer, R. Yu. Barkov, O. A. Yakovtseva, and A. V. Pozdniakov, "Comparative analysis of structure and properties of quasibinary Al–6.5Cu–2.3Y and Al–6Cu–4.05Er alloys," Phys. Met. Metallogr. **121**, 476–482 (2020).
14. A. V. Pozdnyakov, R. Yu. Barkov, Zh. Sarsenbaev, S. M. Amer, and A. S. Prosviryakov, "Evolution of microstructure and mechanical properties of a new Al–Cu–Er wrought alloy," Phys. Met. Metallogr. **120**, 614–619 (2019).
15. T. K. Akopyan, N. V. Letyagin, N. A. Belov, A. N. Koshmin, and D. Sh. Gizatulin, "Analysis of the microstructure and mechanical properties of a new wrought alloy based on the ((Al) + Al4(Ca,La)) eutectic," Phys. Met. Metallogr. **121**, 914–919 (2020).
16. A. V. Pozdnyakov, A. A. Osipenkova, D. A. Popov, S. V. Makhov, and V. I. Napalkov, "Effect of low additions of Y, Sm, Gd, Hf and Er on the structure and hardness of alloy Al–0.2% Zr–0.1% Sc," Met. Sci. Heat Treat. **58**, 537–542 (2017).
17. A. V. Pozdniakov, R. Yu. Barkov, A. S. Prosviryakov, A. Yu. Churyumov, I. S. Golovin, and V. S. Zolotorevskiy, "Effect of Zr on the microstructure, recrystallization behavior, mechanical properties and electrical conductivity of the novel Al–Er–Y alloy," J. Alloys Compd. **765**, 1–6 (2018).
18. A. V. Pozdniakov and R. Yu. Barkov, "Microstructure and mechanical properties of novel Al–Y–Sc alloys

with high thermal stability and electrical conductivity," J. Mater. Sci. Technol. **36**, 1–6 (2020).

19. Y. Zhang, K. Gao, S. Wen, H. Huang, Z. Nie, and D. Zhou, "The study on the coarsening process and precipitation strengthening of Al3Er precipitate in Al–Er binary alloy," J. Alloys Compd. **610**, 27–34 (2014).
20. S. P. Wen, K. Y. Gao, Y. Li, H. Huang, and Z. R. Nie, "Synergetic effect of Er and Zr on the precipitation hardening of Al–Er–Zr alloy," Scr. Mater. **65**, 592–595 (2011).
21. S. P. Wen, K. Y. Gao, H. Huang, W. Wang, and Z. R. Nie, "Precipitation evolution in Al–Er–Zr alloys during aging at elevated temperature," J. Alloys Compd. **574**, 92–97 (2013).
22. Y. Zhang, H. Gao, Y. Kuai, Y. Han, J. Wang, B. Sun, S. Gu, and W. You, "Effects of Y additions on the precipitation and recrystallization of Al–Zr alloys," Mater. Charact. **86**, 1–8 (2013).
23. Y. Zhang, J. Gu, Y. Tian, H. Gao, J. Wang, and B. Sun, "Microstructural evolution and mechanical property of Al–Zr and Al–Zr–Y alloys," Mater. Sci. Eng., A **616**, 132–140 (2014).
24. A. V. Pozdniakov, V. Yarasu, R. Yu. Barkov, O. A. Yakovtseva, S. V. Makhov, and V. I. Napalkov, "Microstructure and mechanical properties of novel Al–Mg–Mn–Zr–Sc–Er alloy," Mater. Lett. **202**, 116–119 (2017).
25. M. Song, K. Du, Z. Y. Huang, H. Huang, Z. R. Nie, and H. Q. Ye, "Deformation-induced dissolution and growth of precipitates in an Al–Mg–Er alloy during high-cycle fatigue," Acta Mater. **81**, 409–419 (2014).
26. H. L. Hao, D. R. Ni, Z. Zhang, D. Wang, B. L. Xiao, and Z. Y. Ma, "Microstructure and mechanical properties of Al–Mg–Er sheets jointed by friction stir welding," Mater. Des. **52**, 706–712 (2013).
27. S. P. Wen, W. Wang, W. H. Zhao, X. L. Wu, K. Y. Gao, H. Huang, and Z. R. Nie, "Precipitation hardening and recrystallization behavior of Al–Mg–Er–Zr alloys," J. Alloys Compd. **687**, 143–151 (2016).
28. R. Yu. Barkov, A. V. Pozdniakov, E. Tkachuk, and V. S. Zolotorevskiy, "Effect of Y on microstructure and mechanical properties of Al–Mg–Mn–Zr–Sc alloy with low Sc content," Mater. Lett. **217**, 135–138 (2018).
29. R. Yu. Barkov, A. G. Mochugovskiy, M. G. Khomutov, and A. V. Pozdniakov, "Effect of Zr and Er small additives on the phase composition and mechanical properties of Al–5Si–1.3Cu–0.5Mg alloy," Phys. Met. Metallogr. **122**, 161–168 (2021).
30. R. Yu. Barkov, A. S. Prosviryakov, M. G. Khomutov, and A. V. Pozdnyakov, "Effect of the Zr and Er content on the structure and properties of the Al–5Si–1.3Cu–0.5Mg alloy," Phys. Met. Metallogr. **122**, 614–620 (2021).
31. M. Li, H. Wang, Z. Wei, and Z. Zhu, "The effect of Y on the hot-tearing resistance of Al–5 wt % Cu based alloy," Mater. Des. **31**, 2483–2487 (2010).
32. A. V. Pozdniakov, R. Yu. Barkov, S. M. Amer, V. S. Levchenko, A. D. Kotov, and A. V. Mikhaylovskaya, "Microstructure, mechanical properties and superplasticity of the Al–Cu–Y–Zr alloy," Mater. Sci. Eng., A **758**, 28–35 (2019).
33. S. M. Amer, R. Yu. Barkov, O. A. Yakovtseva, I. S. Loginova, and A. V. Pozdniakov, "Effect of Zr on microstructure and mechanical properties of the Al–Cu–Er alloy," Mater. Sci. Techol. **36** (4), 453–459 (2020).
34. S. Amer, O. Yakovtseva, I. Loginova, S. Medvedeva, A. Prosviryakov, A. Bazlov, R. Barkov, and A. Pozdniakov "The phase composition and mechanical properties of the novel precipitation-strengthening Al–Cu–Er–Mn–Zr alloy," Appl. Sci. **10** (15), 5345–5353 (2020).
35. S. M. Amer, R. Yu. Barkov, and A. V. Pozdniakov, "Effect of Mn on the phase composition and properties of Al–Cu–Y–Zr alloy," Phys. Met. Metallogr. **121**, 1227–1232 (2020).
36. S. M. Amer, R. Yu. Barkov, and A. V. Pozdniakov, "Effect of impurities on the phase composition and properties of a wrought Al–6% Cu–4.05% Er alloy," Phys. Met. Metallogr. **121**, 495–499 (2020).
37. S. M. Amer, R. Yu. Barkov, and A. V. Pozdniakov, "Effect of iron and silicon impurities on phase composition and mechanical properties of Al–6.3Cu–3.2Y alloy," Phys. Met. Metallogr. **121**, 1002–1007 (2020).
38. S. M. Amer, R. Yu. Barkov, A. S. Prosviryakov, and A. V. Pozdniakov, Fiz. Met. Metalloved. (in press).
39. L. Zhang, P. J. Masset, X. Tao, G. Huang, H. Luo, L. Liu, and Z. Jin, "Thermodynamic description of the Al–Cu–Y ternary system," CALPHAD: Comput. Coupling Phase Diagrams Thermochem. **35**, 574–579 (2011).
40. L. G. Zhang, L. B. Liu, G. X. Huang, H. Y. Qi, B. R. Jia, and Z. P. Jin, "Thermodynamic assessment of the Al–Cu–Er system," CALPHAD: Comput. Coupling Phase Diagrams Thermochem. **32**, 527–534 (2008).
41. *GOST* (State Standard) *21631–76: Sheets of Aluminum and Aluminum Alloys. Specifications* (Standartinform, Moscow, 2008) [in Russian].
42. *GOST* (State Standard) *R 51834–2001: Extruded Aluminum Alloy Bars of High Strength and Improved Ductility. Specifications* (Izd. Standartov, Moscow, 2002) [in Russian].

Translated by N. Kolchugina